THE ASTRONOMICAL JOURNAL, 120:3218–3225, 2000 December
© 2000. The American Astronomical Society. All rights reserved. Printed in U.S.A.

G106.3+2.7: A SUPERNOVA REMNANT IN A LATE STAGE OF EVOLUTION

SERGE PINEAULT[1] AND GILLES JONCAS
Département de Physique and Observatoire du Mont Mégantic, Université Laval, Ste-Foy, PQ G1K 7P4, Canada
Received 2000 June 22; accepted 2000 August 16

ABSTRACT

We report on observations of the candidate supernova remnant (SNR) G106.3+2.7 with the Dominion Radio Astrophysical Observatory's Synthesis Telescope in the continuum at both 408 and 1420 MHz and in the 21 cm line of neutral hydrogen. The general morphology of the object and its spectral index ($\alpha \approx 0.57 \pm 0.04$, where $S_\nu \propto \nu^{-\alpha}$) confirm it as an SNR. The object consists of two distinct components, the head and the tail. The tail component is of lower surface brightness and has a marginally steeper spectral index than the head component. A deficiency of neutral hydrogen at an LSR velocity of about -105 km s^{-1} is most likely due to the effect of the SNR, suggesting that the SNR is expanding at a velocity of about 15 km s^{-1}, it is at a kinematic distance of 12 kpc, and its largest angular extent is of the order of 200 pc. These parameters are shown to be consistent with a dynamical model in which the SNR is in a very late stage of its isothermal evolution, where the pressure inside the SNR is approaching the pressure of the ambient interstellar medium. We also describe the H II region Sh 141, which is about 20′ north of G106.3+2.7.

Key words: H II regions — ISM: H I — ISM: structure — supernova remnants

1. INTRODUCTION

The extended object G106.3+2.7 was discovered by Joncas & Higgs (1990) as part of a radio survey of the northern Galactic plane undertaken at the Dominion Radio Astrophysical Observatory (DRAO). Although the object lies about 1°.5 away from their observational field center, it is clearly visible on their 408 MHz map (being, however, well past the 20% primary beam radius at 1420 MHz), with an estimated integrated flux density of 8.4 ± 0.5 Jy. The object seems to consist of two lobes of irregular outline with a brighter northeast component and a fainter, somewhat more extended, southwest component. In what follows, we shall refer to these components as the head and tail components, respectively. There was a hint of a bridge or plateau of emission linking the two components, but this could simply be the common background on which the two components sit.

Using the 1420 MHz observations of Kallas & Reich (1980), Joncas & Higgs (1990) obtained a total flux of about 4.7 Jy, yielding a spectral index of 0.45 ± 0.05 for the entire object (Kallas & Reich's observations lacked the resolution to separate out the two components). The double-component nature of G106.3+2.7 is also revealed by the 2.7 GHz, 4′.3 observations of Fürst et al. (1990). The position of the object near the Galactic plane, its spectral index, and its general morphology all point to the object's being a previously undiscovered, shell-type supernova remnant (SNR).

Joncas & Higgs (1990) also noted that there was no conspicuous infrared emission associated with the object, strenghtening the SNR interpretation. A quick inspection of the Infrared Sky Survey Atlas seems, however, to show that there is weak emission at both ends of G106.3+2.7. If real, this could be indicative of a buildup of material caused by the expansion of the nebula or from an interaction between the nebula and gas already present (if both are at the same distance). In either case, the IR emission suggests that neutral gas could be present.

Apart from the fact that all of the above observations are at best of moderate resolution and that there is a clear need for higher resolution images of this object, a better knowledge of the morphology, relationship with the surrounding interstellar medium (ISM), and spectral properties of this candidate SNR is important for many reasons.

First, current SNR catalogs (Green 1988, 1998)[2] are known to be incomplete and lacking both large, low surface brightness remnants and small angular size younger remnants, so that it is imperative to obtain as unbiased a sample as possible to draw meaningful statistical inferences. Using a flux density of 8.4 Jy and equivalent angular diameter of 34′ at 408 MHz, the surface brightness of G106.3+2.7 is estimated as $\Sigma_{408} \approx 1.1 \times 10^{-21}$ W Hz^{-1} m^{-2} sr^{-1} or, using the estimated spectral index of 0.45 to convert to a frequency of 1 GHz, $\Sigma_{1\ \mathrm{GHz}} \approx 7 \times 10^{-22}$ W Hz^{-1} m^{-2} sr^{-1}; indeed a relatively low surface brightness object (as a reference, the 2.7 GHz Effelsberg survey [Fürst et al. 1990] is considered complete to $\Sigma_{1\ \mathrm{GHz}} \approx 2 \times 10^{-22}$ W Hz^{-1} m^{-2} sr^{-1}).

Second, because of the position of the object in the second quadrant of the Galaxy, confusion with neutral gas *not* associated with the object should be minimal, thereby facilitating identification of gas possibly associated with the object. Furthermore, the uniqueness of the distance-velocity relationship along this line of sight means that any firm association implies an unambiguous determination of the distance.

Third, if G106.3+2.7 is indeed an SNR, it could very well provide us with an opportunity to confront competing theories of SNR evolution. The particular morphology of the SNR (two nearly disconnected components) appears particularly promising in that respect. One of the simplest explanations is that the expanding remnant has propagated into a highly inhomogeneous ISM, possibly breaking into a

[1] On sabbatical leave at the Dominion Radio Astrophysical Observatory, National Research Council of Canada.

[2] Available at http://www.mrao.cam.ac.uk/surveys/snrs.

low-density cavity just as the SNR DA 174 (Landecker et al. 1982; Pineault, Landecker, & Routledge 1987), maybe the most spectacular such example. Unlike DA 174, however, the breakout in G106.3+2.7 (if indeed there has been a breakout) would have taken place *parallel* to the Galactic plane and not perpendicular to it. However, the morphology of remnants is quite diverse, and an obvious question that arises is the extent to which intrinsic or extrinsic factors are primarily responsible for determining the overall morphology of an SNR. Given its location toward a line of sight relatively free of confusion effects, this candidate SNR offers a good opportunity to further investigate this issue.

2. OBSERVATIONS AND DATA REDUCTION

G106.3+2.7 was observed with the DRAO Synthesis Telescope (ST) operating simultaneously at 408 MHz and 1420 MHz in continuum mode and at 1420 MHz in spectral line mode (H I). The telescope consists of seven 9 m antennas aligned on a 600 m east-west baseline (Landecker et al. 2000). All spacings from a minimum of 12.9 m were observed with a spacing increment of 4.286 m. Table 1 shows the instrumental parameters for the DRAO observations.

Reduction of continuum data from the ST followed conventional lines, including application of the CLEAN and self-calibration algorithms and the application of a correction factor for the effect of the automatic gain control system at 408 MHz. Because of the relative proximity of Cassiopeia A, particular care had to be exercised to properly remove the effect of this source. The still relatively high noise level at 408 MHz is attributable to remaining artifacts from Cas A. The data at both frequencies were registered in position and flux to ensure a proper calibration. This procedure involved the comparison of compact sources with their counterparts in catalogs from previous surveys of similar angular resolution and is described by Taylor et al. (2000). The internal consistency of the data is high, with relative calibration errors of less than 1% in the continuum flux at both frequencies, although an uncertainty of up to 10% may still exist in the absolute 408 MHz flux scale. Positional uncertainties are of order 0.″15 and 0.″20 in right ascension and declination at 1420 and 408 MHz, respectively. The corresponding uncertainties in the H I data are about 3 times higher.

At the time of the observations, the DRAO ST was equipped with 128-channel spectrometers for observations of the 21 cm H I spectral line. The 2′ angular resolution available in the H I line was largely adequate for our purposes (the object's minor-axis size is of the order of 20′). Because of the almost complete coverage of the (u, v)-plane, the sidelobe levels of the unCLEANed beam were low (-2% at a radius of 2′), and it was not necessary to CLEAN the H I maps. The 128 H I images were inspected, and end channels free of H I emission (between 42 and 54 km s^{-1} at one end and -140 and -152 km s^{-1} at the other end) were averaged to form a continuum map that was then subtracted from each channel map to remove continuum emission. All maps shown have had the continuum so removed, and all velocities are with respect to the local standard of rest (LSR).

The DRAO ST cannot observe on baselines shorter than 12.9 m, and it therefore loses sensitivity to structure of large angular scale. Single-antenna observations were used to provide information on such structure. For the continuum, the 1420 MHz Effelsberg survey (Kallas & Reich 1980) and the 408 MHz all-sky survey from Haslam et al. (1982) were used. For the H I line maps, low-resolution images were obtained with the 26 m DRAO telescope. A detailed description of the spatial filtering process used to add the low-resolution and Synthesis Telescope observations can be found in Joncas & Higgs (1990) or Normandeau, Taylor, & Dewdney (1997).

3. RESULTS

3.1. *Radio Continuum Data*

Figure 1 shows the continuum radio emission at 1420 MHz. The general morphology of the object, in particular its double-component structure, is obvious, and new interesting features are revealed. The head component appears to consist of separate knots of intense radio emission. One

TABLE 1

SYNTHESIS TELESCOPE OBSERVATIONAL PARAMETERS

Parameter	408 MHz	1420 MHz
Calibrators and assumed fluxes:[a]		
3C 147	48 Jy	21.3 Jy
3C 295	54 Jy	...
Received polarization	Right circular	Left circular
Field of view (to 50%)	5.°3	1.°7
Field of view (to 20%)	8.°1	2.°6
Grating ring radii (N-S × E-W)	9.°9 × 9.°9	2.°8 × 2.°8
Continuum:		
Bandwidth[b]	4 MHz	15 MHz
Synthesized beam (N-S × E-W)	3.′92 × 3.′49	1.′15 × 1.′0
Observed rms noise	6.9 mJy beam^{-1}	0.24 mJy beam^{-1}
H I spectral line:	...	
Synthesized beam (N-S × E-W)	...	2.′3 × 2.′0
Observed rms noise (single channel)	...	1.4 K
Channel width	...	1.649 km s^{-1}
Velocity resolution	...	2.64 km s^{-1}
Velocity coverage	...	+55 to −155 km s^{-1}

[a] Fluxes consistent with the scale of Baars et al. 1977.

[b] The 1420 MHz continuum bandpass excludes H I emission.

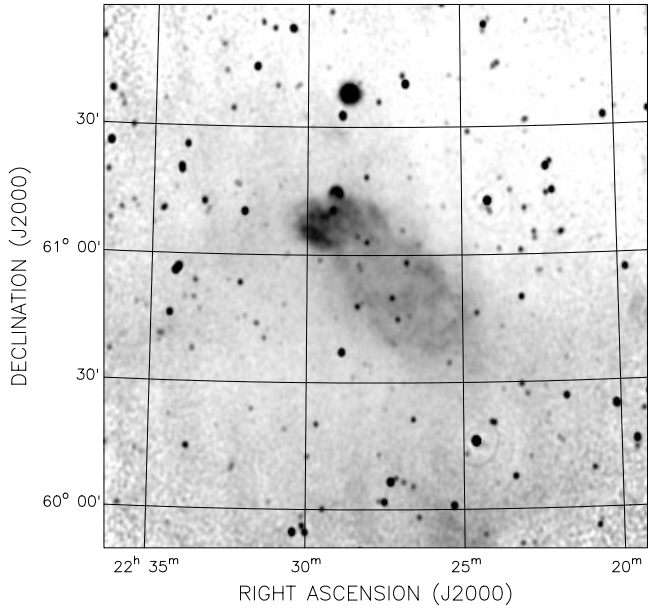

FIG. 1.—Brightness temperature map of the 1420 MHz radio continuum emission corrected for primary-beam attenuation. Shadings run smoothly from 6 K (*white*) to 9 K (*black*). Resolution is 1.′15 × 1.′0 (north-south by east-west). The strong source Cas A, at $\alpha \approx 23^h23^m$, $\delta \approx 58°48'$ (or $l \approx 112°$, $b \approx -2°$), is located about 7° to the southeast of the map center.

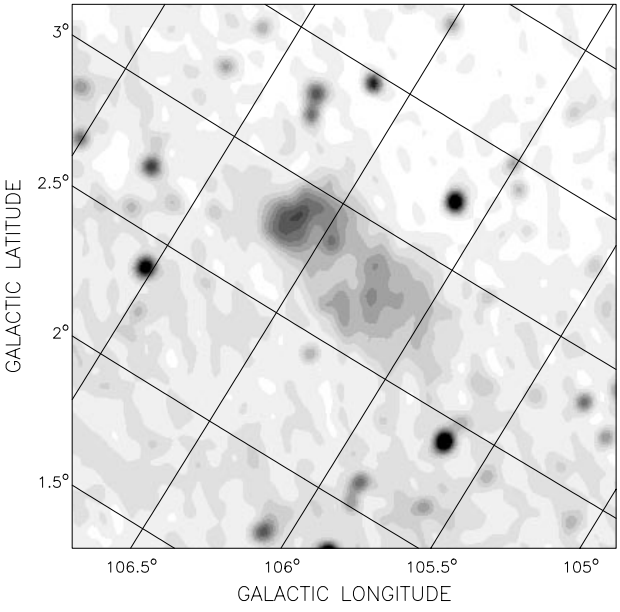

FIG. 2.—Same as Fig. 1, but at 408 MHz. Gray scale steps occur from 60 K to 125 K by steps of 6.5 K. Resolution is 3.′92 × 3.′49 (north-south by east-west).

of these, to the north, has a boomerang-like shape and could be an extragalactic head-tail radio galaxy barely resolved by the DRAO ST. However, as will be seen shortly, its spectral index does not differ much from the value found for the object as a whole. The brightest part of the tail component has a broken shell appearance superposed on a lower level background emission extending to the southwest past the brighter parts. Although the precise size of the object is not well defined at this frequency, it can be described as an oblong object of rough dimensions 60′ × 24′. A number of compact, likely extragalactic, sources are seen projected on the object.

Figure 2 shows the corresponding map at 408 MHz. The same general features seen at 1420 MHz are also present here, although the resolution is much lower. The dimension of the source appears to be better defined at this lower frequency, suggesting that a large part of the background emission is thermal in nature. The mottled appearance of the map (and, consequently, substantially higher noise) is a result of some remaining artifacts caused by the strong source Cas A.

To obtain more quantitative properties for G106.3+2.7, we proceeded to determine the spectral index of different parts of the object. As a first step, all of the bright compact sources were removed by fitting two-dimensional Gaussians to the map data at both frequencies, making sure that a smooth background was left. Both maps were then convolved to a common resolution of 4′ × 4′ (close to the full resolution at 408 MHz).

Spectral indices were computed using the method of *T-T* plots, in which the brightness temperature at one frequency is plotted point by point against the brightness temperature at the other frequency, the spectral index being determined from the slope of a straight line fitted by regression (see e.g., Pineault et al. 1997). Indices were determined separately for the head and tail components, as well as for the whole object. The obtained values and their errors derived from the fitting procedure are shown as α_{TT} in Table 2. There is an indication that the spectral index of the tail component is slightly steeper. We also carried out the same procedure for the head component but excluded the region of the boomerang-like feature. The value obtained was then 0.57 ± 0.04, suggesting that the boomerang-shaped feature has a somewhat flatter spectral index than the body of the head component.

Integrated flux densities were also estimated by fitting twisted-plane base levels to the vertices of polygons enclosing the emission region (on maps with the compact sources removed). The derived flux densities are very sensitive to the definition of base levels and are therefore rather imprecise, as are the spectral indices α_{int} derived from them. These values are also shown in Table 2. The quoted values and their errors are based on the average and standard deviation of three separate determinations. Because of the poorer resolution at 408 MHz, it is likely that many compact sources that could not be removed contribute to the integrated flux density at that frequency. However, we estimate that the overestimated flux density and resulting spectral steepening are negligible compared with the quoted errors.

Both methods of spectral index determination yield values typical for shell SNRs (the average is about 0.5; Lozinskaya 1992, p. 257), and hereafter we adopt this interpretation. We inspected our two maps for the presence of an

TABLE 2

INTEGRATED FLUX DENSITIES AND SPECTRAL INDICES

Object	S_{1420}	S_{408}	α_{int}	α_{TT}
Head	2.3 (0.3)	4.7 (0.3)	0.56 (0.10)	0.49 (0.05)
Tail.....	2.6 (0.4)	5.7 (0.2)	0.63 (0.11)	0.70 (0.07)
Whole.....	4.9 (0.6)	10.5 (0.3)	0.61 (0.09)	0.57 (0.04)

NOTE.—Errors shown in parentheses.

unusual compact source, i.e., one having a peculiar spectrum and/or privileged position. One source is present on both maps near $\alpha \approx 22^h28^m$ and $\delta \approx 61°3'$ on Figure 1. By comparing the two maps, it is apparent, however, that the source on the lower resolution 408 MHz map is in fact a blend of three separate sources seen at 1420 MHz. The spectral index of this blend is 1.47, which suggests that the brighter source is a steep-spectrum extragalactic object.

Finally, the bright and slightly extended circular source seen directly to the north of G106.3+2.7 at $\alpha \approx 22^h29^m$, $\delta \approx 61°35'$ is the H II region Sh 141 (Sharpless 1959). Its measured flux density is 560 ± 20 Jy at 1420 MHz and 500 ± 50 Jy at 408 MHz, giving a spectral index of -0.09 ($S_\nu \propto \nu^{-\alpha}$). It is well fitted by a circular Gaussian of width 3.2. The compact source located about 5′ to the south-southeast of Sh 141 has a spectral index of 0.95 and is likely extragalactic. Fich & Blitz (1984) detected a -65 km s^{-1} CO cloud near Sh 141, while Fich, Treffers, & Dahl (1990) measured an Hα line at -63.8 km s^{-1}. Both velocities are with respect to the LSR. These velocities imply a kinematic distance of about 7 kpc using a flat rotation curve model with $V_0 = 220$ km s^{-1} and $R_0 = 8.5$ kpc. Providing that Sh 141 is a spherical H II region, the relations given by Schraml & Mezger (1969) can be used to derive the excitation parameter of the object. Thereupon the models of Panagia (1973) indicate that Sh 141 could be excited by a single O8 star.

3.2. *Infrared Data*

As a next step, we obtained infrared maps in the form of high resolution processed (HIRES; Fowler & Aumann 1994) *IRAS* images. The 60 μm and 100 μm maps were part of the *IRAS* Galaxy Atlas produced by Cao et al. (1997) at the Infrared Processing and Analysis Center.[3] The 12 μm and 25 μm Mid-Infrared Galaxy Atlas images were processed by Kerton & Martin (2000). The images used are the result of 20 iterations of the algorithm, giving an approximate resolution ranging from about 0.5 at 12 μm to about 2′ at 100 μm. The maps in all four bands were carefully inspected. Figure 3 presents the 60 μm map of the same field as shown for the radio continuum. Apart from bright unrelated features far to the west of the SNR and the bright H II region Sh 141 to the north, the infrared and radio continuum maps show very little correlation. IR emission is somewhat higher near the head component and to the west of the tail, and a relatively conspicuous IR deficiency is apparent to the south and east of the SNR. The lack of distinctive features associated with the SNR is a likely indication that no significant amount of dust has been heated by the SNR and/or that the ambient dust has had time to cool.

3.3. *DRAO Neutral Hydrogen Data*

Figure 4 shows the average H I spectrum in a circular area of diameter 100′ around the phase center of the observation. This spectrum is typical of the emission in this vicinity, as can be seen from the H I survey of Weaver & Williams (1973). All individual maps were carefully inspected and compared with the radio continuum map to find evidence of interaction of the SNR with the ambient ISM. To increase the signal-to-noise ratio, adjacent channels were averaged 3 × 3, bringing the rms noise near the map center to 0.81 K. The spectral resolution was then about 5 km s^{-1}.

Figure 5 is a subset of the three-channel average maps, showing details of the H I emission on all scales, from the broadest emission regions to the finest detail allowed by the resolution limit. With the exception of the range from +10 to -25 km s^{-1}, corresponding to the local H I gas, only channels with significant emission and features readily distinguishable from the general background are presented. Each map has had a baseline subtracted equal to the average H I level in the 100′ diameter central region in that velocity range. This does not distort the H I structure in the

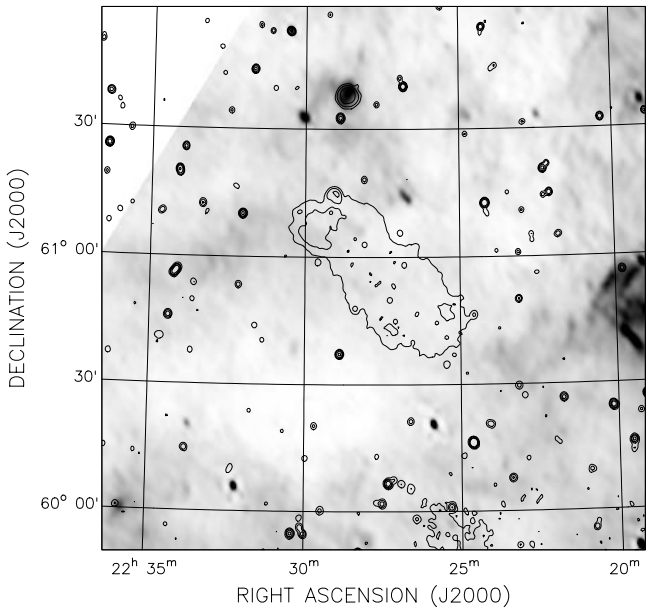

FIG. 3.—HIRES 60 μm map. Shadings run smoothly from 13 MJy sr^{-1} (*white*) to 64 MJy sr^{-1} (*black*). Contours of the radio continuum emission at 1420 MHz are superposed for values of the brightness temperature of 7, 8, 10, and 14 K.

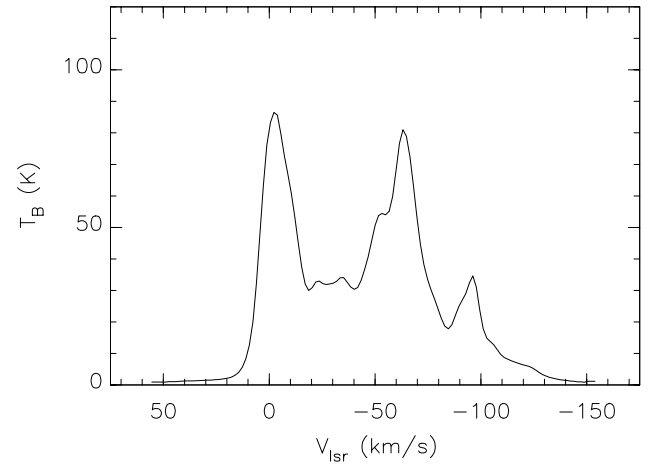

FIG. 4.—Average neutral hydrogen spectrum over a region of diameter 100′ centered on G106.3+2.7.

[3] The Infrared Processing and Analysis Center is funded by NASA as part of the *Infrared Astronomical Satellite* extended mission under contract to the Jet Propulsion Laboratory.

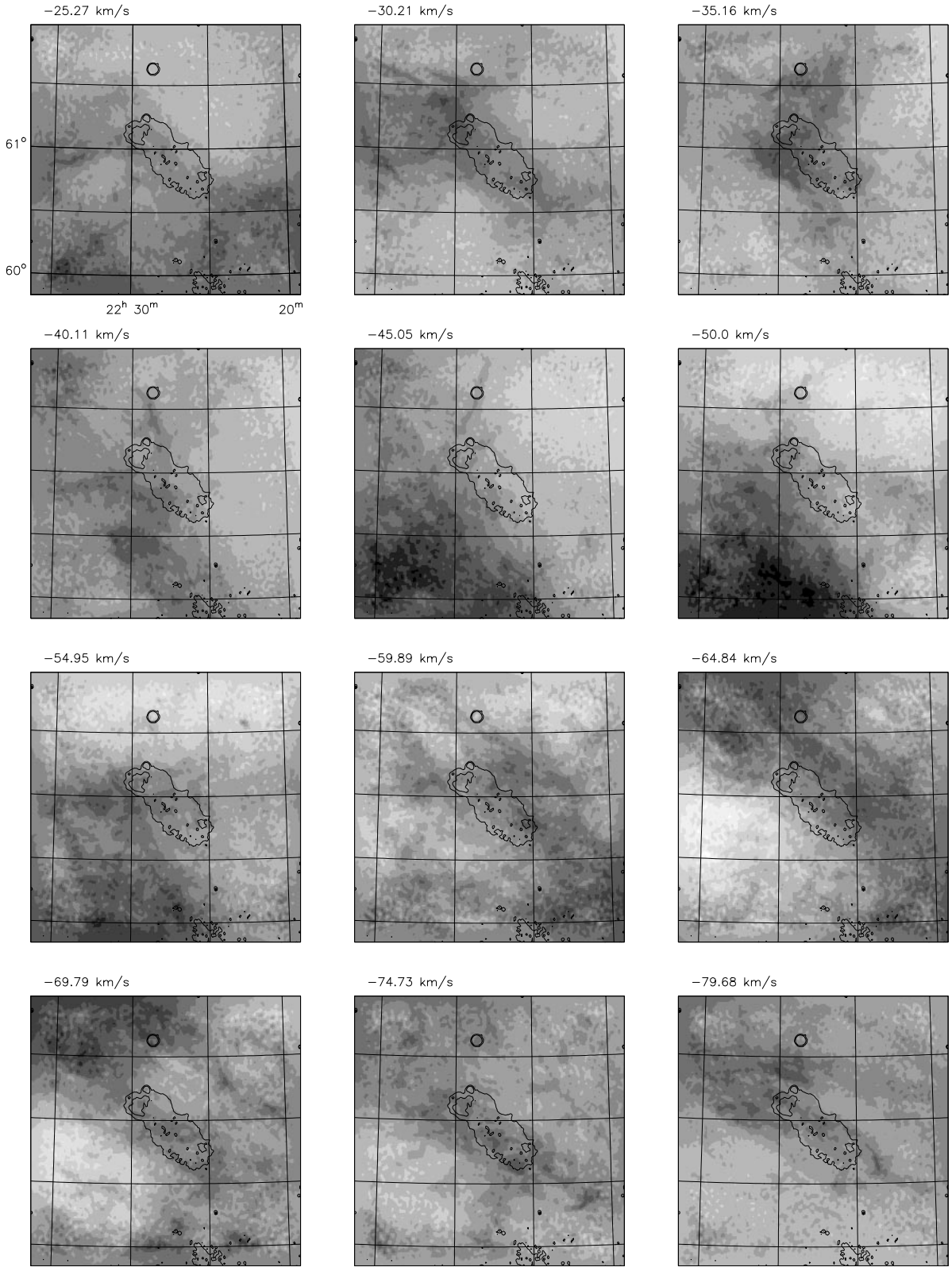

FIG. 5.—Gray-scale representation of neutral hydrogen emission. Velocity resolution is 5 km s^{-1}. The central LSR velocity of each frame is indicated at the top left corner. Gray-scale transitions are from -40 to $+40$ K in steps of 8 K relative to the average brightness temperature in the field at this velocity. The average temperature can be read from the previous figure. A J2000.0 equatorial coordinate grid (reference values can be seen on the top left panel) and a few 1420 MHz continuum contours (from an image where point sources have been removed) have been overlaid on each map.

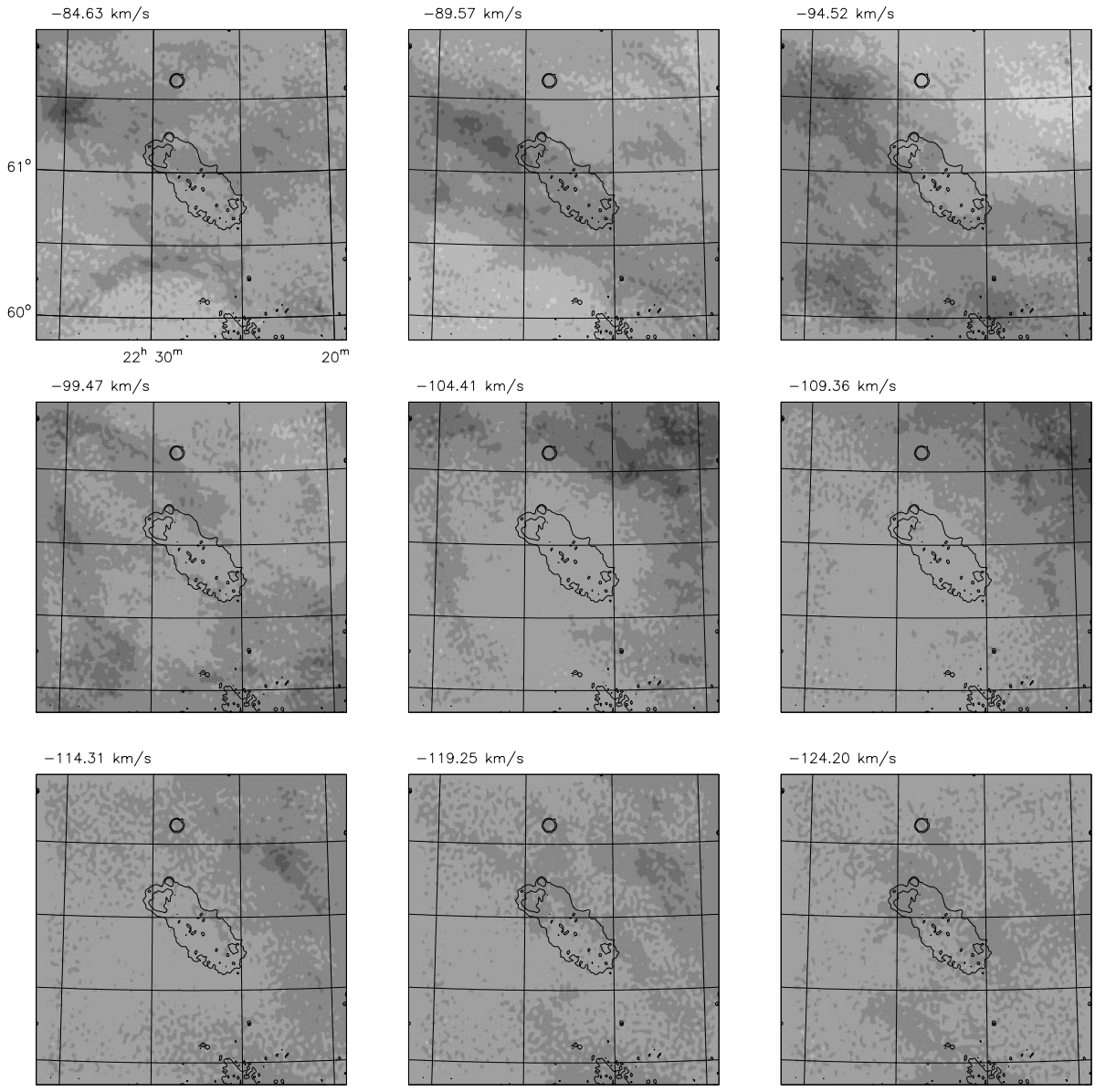

FIG. 5.—*Continued*

maps but simply reduces the dynamic range required for their display. The amount subtracted from each map can be read off the spectrum of Figure 4. For comparison, a few contours of the 1420 MHz continuum emission have been superposed on each line map.

Evidence of interaction of the SNR with the ambient ISM can take the form of a deficiency of neutral hydrogen at the position of the SNR and/or high-velocity (with respect to the SNR systemic velocity) accelerated clouds. For the type of interaction of the first case to be credible in the case of an SNR, the H I deficiency should be visible over many channels, typically over a range of at least 10 to 15 km s^{-1}.

Inspection of Figure 5 shows a deficiency of H I at the position of the SNR at about -104 km s^{-1}, where the "hole" size appears to be maximum. This lack of H I can be traced back toward both smaller and larger velocities, to about -94 and -124 km s^{-1}, respectively, thus spanning a range of about 30 km s^{-1}. If this feature is indeed associated with the SNR, we deduce a current expansion velocity of about 15 km s^{-1}.

As mentioned in § 3.1, the H II region Sh 141 is associated with a -65 km s^{-1} CO cloud. Therefore, the radiation field of the ionizing star will create a photodissociated H I interface between the H II region and the CO cloud, which should be prominent with respect to the local H I background. However, the neutral hydrogen maps of Figure 5 do not show any enhanced H I emission in the velocity range covered by the CO cloud and the H II region (we have also inspected the single-channel maps with the same result). In addition, there is no trough of H I emission at the velocity of the ionized gas (-63.8 km s^{-1}) as expected from the action of an ionizing star (e.g., Joncas et al. 1985). This situation may result from a combination of object geometry and instrumental limitations. If Sh 141 is seen face-on (as for the Orion Nebula), this would explain the absence of a trough because the telescope would be unable to discern the enhanced emission from the photodissociated H I as a result of inadequate contrast. If Sh 141 is seen edge-on, the DRAO ST lacks the spatial resolution ($1' = 2$ pc) to detect the photodissociated H I interface. The maximum thickness of

the interface when an O8 star is present near a molecular cloud with a mean density of 300 cm^{-3} is 1 pc (Roger & Dewdney 1992). If G106.3+2.7 was at the same distance as the H II region, we would also expect a signature of the interaction in the H I data, which is clearly not the case.

4. DISCUSSION AND CONCLUSIONS

In this section, we show that it is possible to obtain a self-consistent model for G106.3+2.7. Any dynamical model of an SNR requires a knowledge of the actual key physical parameters of the object, in particular its true physical diameter, which, in turn, requires the distance to be known. Unfortunately, SNR distance determination is an exercise fraught with uncertainties. Use of a surface brightness–diameter (Σ-D) relation is considered unreliable (Green 1985), although Berkhuijsen (1986) has shown that such a relation still holds if D is taken as the *maximum* allowed diameter. Using the 408 MHz flux of 10.5 Jy (Table 2), a mean spectral index of 0.57, and equivalent diameter of 50′ for the SNR, we obtain a maximum diameter of 165 pc, corresponding to a maximum distance of 11.5 kpc. This maximum distance turns out to be consistent with the kinematic distance that we obtain by using a flat rotation curve model with $R_o = 8.5$ kpc and $V_o = 220$ km s^{-1} and assuming the systemic velocity of the SNR to be -104 km s^{-1} (in accordance with the neutral hydrogen results of the previous section).

We now discuss the dynamics of the SNR, adopting 12 kpc as its distance. The various phases of the expansion of an SNR have been conveniently summarized by Lozinskaya (1992, p. 205). We assume the SNR has reached the isothermal phase (which is largely shown to be the case below), for which the relevant dynamical equations are

$$R_s = 38(\epsilon E_{51}/n_0)^{5/21} t_5^{2/7} \text{ pc} , \quad (1)$$

$$t_5 = [R_s/(38 \text{ pc})]^{7/2} (\epsilon \mathrm{E}_{51}/\mathrm{n}_0)^{-5/6} , \quad (2)$$

where $\epsilon \equiv E_T/E_0$ is the ratio of thermal to total energy (of the order of 0.2 to 0.35), t_5 is the SNR age in units of 10^5 yr, n_0 is the ambient particle number density in which the SNR is expanding, $E_{51} = E_0/10^{51}$ ergs, and R_s is the SNR shell radius.

With the SNR being asymmetric, its radius is not uniquely defined, so we adopt a mean value of 20′ for its angular radius, which translates to a physical radius of 70 pc for an assumed distance of 12 kpc. We take $\epsilon = 0.27$ and keep E_{51} and n_o as free parameters. Setting $R_s = 70$ pc in equation (2) yields an age of $t_5 = 25.3(n_0/E_{51})^{0.83}$ for the SNR. The neutral hydrogen structure, which we have suggested to be associated with the SNR, covers a velocity range of about 30 km s^{-1}, so we assume the SNR shock velocity is 15 km s^{-1}. The velocity follows from the above equation for R_s, $v_s \equiv dR_s/dt = \frac{2}{7}(R_s/t)$, which yields

$$v_s = 7.8(n_0/E_{51})^{-0.83} \text{ km s}^{-1} . \quad (3)$$

A velocity of 15 km s^{-1} obtains for $(n_0/E_{51})^{0.83} = 0.5$, or $n_0 = 0.43E_{51}$ cm^{-3}, yielding $t_5 \approx 12.6$ for the SNR age.

Taken at face value, this age implies that G106.3+2.7 is a relatively old remnant, which might explain the lack of strong limb brightening. To estimate whether such a remnant could already have dissipated, following McKee & Ostriker (1977), we derive the maximum radius R_{max} attained by the SNR as being that at which the gas pressure inside the remnant is balanced by the pressure P_0 of the ambient interstellar gas. This radius and the corresponding time are given by

$$R_{max} = 55E_{51}^{0.32} n_0^{-0.16} \tilde{P}_{04}^{-0.20} \text{ pc} , \quad (4)$$

$$t(R_{max}) = 8.3 \times 10^5 E_{51}^{0.31} \mathrm{n}_0^{0.27} \tilde{P}_{04}^{-0.64} \text{ yr} , \quad (5)$$

where $\tilde{P}_{04} = P_0/10^4 k$ and k is Boltzmann's constant. Substituting for $(n_0/E_{51})^{0.83} = 0.5$ and rounding off some exponents (errors never exceed 0.04), we obtain

$$t(R_{max}) \approx 6.6 \times 10^5 (E_{51}/\tilde{P}_{04})^{0.60} \text{ yr} , \quad (6)$$

$$R_{max} = 63(\mathrm{E}_{51}/\tilde{P}_{04})^{0.20} \text{ pc} . \quad (7)$$

Given the uncertainties in the determination of some key parameters and the fact that the relatively large Galactic latitude and distance imply that G106.3+2.7 is located well away from the midplane at about $z = 580$ pc, we believe that our results are consistent with the object's being an SNR in the late phases of its isothermal evolution. Note that the time for complete dissipation (as opposed to reaching pressure equilibrium with the surrounding ISM) is about 1 order of magnitude larger than $t(R_{max})$ (McKee & Ostriker 1977).

Although G106.3+2.7 may appear anomalously large for an SNR, a quick inspection of Green's (1998) SNR catalog shows that G166.2+2.5 (also known as OA 184), if located at its kinematic distance of about 8 kpc (Routledge, Landecker, & Vaneldik 1986), has a physical size of about 210 pc by 160 pc, i.e., larger than G106.3+2.7 (its minor dimension is substantially larger).

Since a neutron star or black hole is expected to form in the aftermath of a supernova explosion, we have searched existing pulsar catalogs (e.g., Taylor, Manchester, & Lyne 1993). The nearest such object is PSR J2229+6205 (B2227+61) at $l = 107.^\circ2$ and $b = 3.^\circ6$ (it is just off the northern part of the 1420 MHz map shown in Fig. 1). Its dynamical age is about 3×10^6 yr. From its dispersion measure, its distance is estimated as 5.56 kpc. Although this is essentially half of the presumed distance to the SNR, if we suppose for the sake of the argument that the pulsar is at the distance of the SNR, we can evaluate the tangential velocity the pulsar would need to have if it originated from the supernova explosion that gave rise to G106.3+2.7. The angular separation between the pulsar and the bright head component is about 1°, which corresponds to about 200 pc at a distance of 12 kpc. If we use the pulsar dynamical time as the elapsed time, we require a tangential velocity of about 65 km s^{-1}. Taking 10^6 yr (closer to the SNR dynamical time) requires about 200 km s^{-1}. Given that pulsars are known high-velocity objects, the possibility of an association cannot be entirely ruled out, if one is willing to admit a significant error in either distance determination.

In conclusion, the spectral indices of either component or of the object as a whole are wholly consistent with G106.3+2.7 being a shell-type SNR in its late stage of isothermal evolution. There is some weak indication that the tail component could have a slightly steeper spectral index. This could be taken as evidence that the head and tail components are separate objects. Alternatively, it could indicate, although it does not require, that this component represents a region where the shock wave from the SNR has broken into a region of lower density. Pineault et al. (1997) have presented a model for CTA 1 in which the breaking out of the SNR can explain both the lower surface bright-

ness and the spectral index steepening. In the case of G106.3+2.7, the brighter parts of the tail component (Fig. 1) can be taken as having the rough appearance of a weak shell breaking into separate fragments, with more diffuse emission being visible outward. What is clearly required to confirm or refute this hypothesis is better observations (either at 408 MHz or at a much higher frequency, such as 4.8 GHz) at a resolution and sensitivity comparable to our 1420 MHz map so that the spectral index can be mapped more accurately over the remnant. Higher angular resolution observations are also needed to determine whether the boomerang-like feature within the head component is an extragalactic source seen in projection within the SNR or an integral part of the SNR.

This work was supported by the Natural Sciences and Engineering Research Council of Canada and the Fonds FCAR of Québec. The DRAO Synthesis Telescope is operated by the National Research Council of Canada as a national facility. We thank Steve Gibson for carrying out the position and flux registration procedure of the DRAO interferometer maps. S. P. thanks the DRAO for its hospitality during the late stages of this work.

REFERENCES

Baars, J. W. M., Genzel, R., Pauliny-Toth, I. I. K., & Witzel, A. 1977, A&A, 61, 99
Berkhuijsen, E. M. 1986, A&A, 166, 257
Cao, Y., Terebey, S., Prince, T. A., & Beichman, C. A. 1997, ApJS, 111, 387
Fich, M., & Blitz, L. 1984, ApJ, 279, 125
Fich, M., Treffers, R. R., & Dahl, G. P. 1990, AJ, 99, 622
Fowler, J. W., & Aumann, H. H. 1994, in Science with High-Resolution Far-Infrared Data, ed. S. Terebey & J. Mazzarella (JPL Publ. 94-5) (Pasadena: JPL), 1
Fürst, E., Reich, W., Reich, P., & Reif, K. 1990, A&AS, 85, 691
Green, D. A. 1985, MNRAS, 216, 691
———. 1988, Ap&SS, 148, 3
———. 1998, A Catalogue of Galactic Supernova Remnants (Cambridge: Mullard Radio Astrophys. Obs.)
Haslam, C. G. T., Salter, C. J., Stoffel, H., & Wilson, W. E. 1982, A&AS, 47, 1
Joncas, G., Dewdney, P. E., Higgs, L. A., & Roy, J. R. 1985, ApJ, 298, 596
Joncas, G., & Higgs, L. A. 1990, A&AS, 82, 113
Kallas, E., & Reich, W. 1980, A&AS, 42, 227
Kerton, C. R., & Martin, P. G. 2000, ApJS, 126, 85
Landecker, T. L., et al. 2000, A&AS, 145, 509
Landecker, T. L., Pineault, S., Routledge, D., & Vaneldik, F. 1982, ApJ, 261, L41
Lozinskaya, T. A. 1992, Supernovae and Stellar Wind in the Interstellar Medium (New York: AIP)
McKee, C. F., & Ostriker, J. P. 1977, ApJ, 218, 148
Normandeau, M., Taylor, A. R., & Dewdney, P. E. 1997, ApJS, 108, 279
Panagia, N. 1973, AJ, 78, 929
Pineault, S., Landecker, T. L., & Routledge, D. 1987, ApJ, 315, 580
Pineault, S., Landecker, T. L., Swerdlyk, C. M., & Reich, W. 1997, A&A, 324, 1152
Roger, R. S., & Dewdney, P. E. 1992, ApJ, 385, 536
Routledge, D., Landecker, T. L., & Vaneldik, F. 1986, MNRAS, 221, 809
Schraml, J., & Mezger, P. G. 1969, ApJ, 156, 269
Sharpless, S. 1959, ApJS, 4, 257
Taylor, A. R., et al. 2000, in preparation
Taylor, J. H., Manchester, R. N., & Lyne, A. G. 1993, ApJS, 88, 529
Weaver, H., & Williams, D. R. W. 1973, A&AS, 8, 1